

## Study on computational methods applied to modelling of pulse shaper in split-Hopkinson bar

P. BARANOWSKI<sup>1</sup>), J. JANISZEWSKI<sup>2</sup>), J. MALACHOWSKI<sup>1</sup>)

<sup>1</sup>) *Faculty of Mechanical Engineering  
Military University of Technology  
Gen. Kaliskiego 2, 00-908 Warsaw, Poland  
e-mails: pbaranowski@wat.edu.pl,  
jerzy.malachowski@wat.edu.pl*

<sup>2</sup>) *Faculty of Mechatronics and Aviation  
Military University of Technology  
Gen. Kaliskiego 2, 00-908 Warsaw, Poland  
e-mail: jacek.janiszewski@wat.edu.pl*

THE PAPER PRESENTS A POSSIBILITY OF NUMERICAL MODELLING of a copper shaper utilized in an SHPB device with additional attention paid to the proper bar-shaper interaction simulation. The pulse shaper was modelled with the use of three methods available in the commercial code, i.e., applying typical finite Lagrangian elements, meshless smoothed particle hydrodynamics (SPH) method and multi-material arbitrary Lagrangian–Eulerian (MM-ALE) formulation. Additionally, the authors performed a mesh (particles) sensitivity study and the assessment of its influence on the obtained incident pulse characteristics. Consequently, the results obtained from all numerical analyses were compared and validated with the experimental ones with a particular attention given to the shape of the incident pulse and copper shaper deformation. The paper describes also the investigation of a relationship between the contact (coupling) force and the impulse shape.

**Key words:** SHPB, copper shaper, numerical contact, FE analysis, experimental testing.

Copyright © 2014 by IPPT PAN

### 1. Introduction

ONE OF THE MOST POPULAR DEVICES for investigating dynamic behaviour of solid materials at high strain rates within the range of  $10^2$  to  $10^4$  s<sup>-1</sup> [1–11] is a Kolsky bar, more commonly known as the split Hopkinson bar named after Bertram Hopkinson. However, it was John Hopkinson who first investigated stress wave propagation in a wire [2, 12]. Based on the results of his investigations, Bertram (his son) developed a method for recording the movement of a cylinder under strongly dynamic conditions [3, 13]. In 1948, Davies improved this technique with better accuracy of measured data [14], whereas Kol-

sky modified the device and implemented two elastic bars, instead of one, with the investigated specimen placed between them [15]. Since then, this device has been known as the split Hopkinson pressure bar (SHPB) or the Kolsky bar.

The aforementioned SHPB is used for obtaining stress-strain curves of investigated materials for certain strain rates. However, such investigations are exposed to the problems of oscillations recorded by the strain gauges (e.g., Pochhammer–Chree oscillations [14, 16]), which adversely affect the results. The oscillations are the result of wave dispersion. Since the bar material is free to move in the radial direction, the actual stress wave in the bars is two-dimensional. These two-dimensional effects result in dispersion of the wave when it propagates along the slender bars. The effects of dispersion accumulate as the waves propagate over a distance and become more significant when a bar diameter increases as compared to the wavelength.

In an SHPB experiment, the rectangular pulse generated by the impact of the striker on the incident bar is composed of a spectrum of frequencies. Each frequency component has its own propagating velocity. The lag between the higher and lower frequency components of the pulse results in a distorted waveform after traveling a distance. The wave dispersion can be physically minimized by adjusting the incident pulse shape, which directly influences material behaviour [1, 5, 17–20]. The incident pulse can be shaped using several techniques, e.g., by inserting a preloading bar [1, 19, 21], modifying a shape of the striker bar [22, 23–28] or using a small piece of material (so-called pulse shaper) as the mechanical filter which is placed on the impact end of the incident bar. The last mentioned technique is the aim of the authors' study.

In all three cases, numerical correction of the wave dispersion is not needed. The use of the pulse shaping technique extends also the rise time in the incident pulse, which is necessary to achieve stress equilibrium in the specimen [1, 5, 17–20, 29–32].

It should be noted, however, that for different test conditions it is recommended to adjust thickness and a diameter of the pulse shaper [19]. Also, work-hardening or brittle materials need a different thickness-length proportion of the disc. Moreover, as it is presented by other authors [33, 34], effect like friction, apart from others, influences the proper estimation of material properties using SHPB. The authors are aware of all above facts; however, the main aspect of the paper is an attempt to numerically model a copper shaper using different techniques with special attention given to the proper bar-shaper interaction simulation.

In experimental conditions, the use of the pulse shaper is a simple procedure; however, to obtain constant strain rate conditions during tests, many attempts have to be carried out. This is possible to be easily achieved by using numerical methods, more particularly the finite element method, which was presented in other papers [28–33].

However, in the current paper, the authors present the possibility of numerical modelling of a pulse-shaper deformation using three different methods: typical finite Lagrangian elements, meshless smoothed particle hydrodynamics (SPH) method and multi-material arbitrary Lagrangian–Eulerian (MM-ALE) formulation. Additionally, the authors performed a mesh (particles) density sensitivity study with the assessment of its influence on the obtained incident pulse characteristics and copper shaper behaviour during dynamic compression. Consequently, the results obtained from all numerical analyses were compared and validated with the experimental ones with the particular attention pointed to the incident pulse shape and copper shaper deformation. It should be stated that such a concept of shaper modelling using a meshless method (more particularly SPH) and a coupling approach (MM-ALE), besides FE modelling, seems to be novel and original. The authors have not come across any similar work that would cover the study of different methods of wave shaper modelling and their experimental validation.

It should be also noted that one of the main aspects of the study was to emphasize the importance of a correct contact procedure, which is one of the most essential parameters in such investigations. As a consequence, the relationship between the interaction force and the impulse shape was investigated and presented in all cases.

The paper presents a part of wider investigations which aim at finding an optimal shape of an incident pulse for a specific type of material (brittle, ductile or soft). This can be obtained using a discussed shaper or with the special shape of the striker, which in fact was the subject of authors' investigation in their previous paper [28].

## **2. Coupling problem in terms of shaper and bar interaction modelling**

The main problem of the presented study was to properly simulate the interaction between the shaper and bars using three different methods. As it will be presented further, a contact procedure between the aforementioned bodies is especially important in obtaining the expected shape of the incident pulse, which consequently gives the possibility to achieve a proper material characteristic of the material tested in SHPB apparatus. It is known that a pulse shaper reduces the wave dispersion and oscillations of an incident pulse [1, 5, 17–20], as well as it extends the rise time, which is necessary to achieve the stress equilibrium in the specimen [1, 5, 17–20, 29–32]. However, what happens, from the mechanical point of view, when the shaper strikes the bar and during a “severe” impact between the bars? The schema of the contact force in both situations is presented in Fig. 1, which provides a summary of a discussed phenomenon. Not only the

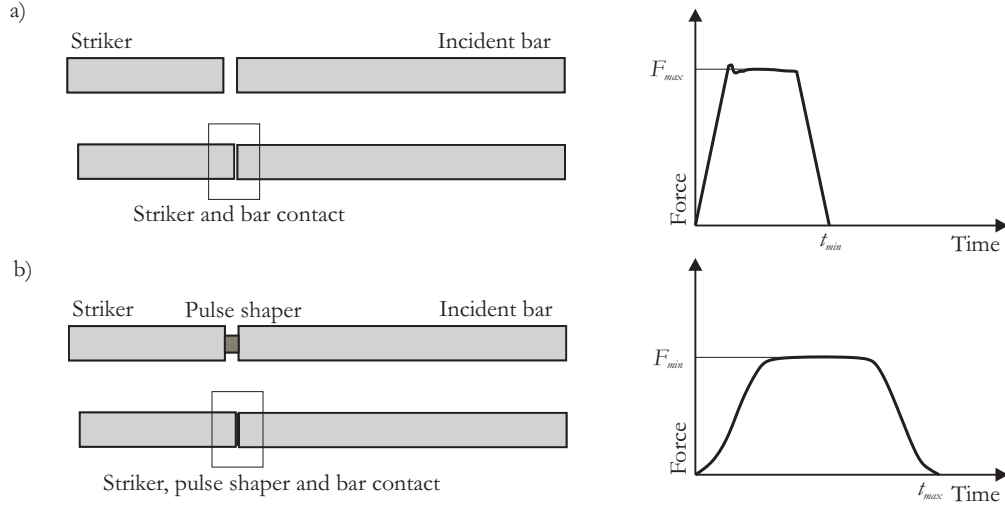


FIG. 1. Contact force in a) "severe" striker-bar impact, b) striker-shaper-bar impact.

amplitude of the impulse of contact force is different but also the shaper operates as a "damper" and its compression results in the impulse extension.

One of the objectives of the study is to emphasize the role of the contact procedure which is the basis for obtaining a proper result, namely the incident impulse shape. Therefore, in the subsequent chapters, a direct relationship between the contact (coupling) force and the impulse shape will be confirmed.

### 2.1. Contact description between interacting bodies

As it was mentioned, one of the most important issues of the paper is an accurate numerical description of the two interacting bodies. The presented computational investigations were based on the analytical considerations included in papers [35, 36].

It was assumed that in the performed analyses the following constitutive relations between contacting bodies are formulated, according to contact normal stress tensor, using penalty method:

$$(2.1) \quad \bar{\mathbf{t}} = \bar{t}_N \bar{\mathbf{n}},$$

where  $t_N = \varepsilon_N g_N$  and  $\varepsilon_N$  is the normal penalty factor.

From the finite element formulation, the contact contribution for slave node  $k$  is formulated based on the following equation:

$$(2.2) \quad C_c^k = \delta \mathbf{u}_c^T \mathbf{F}_c = \delta \mathbf{u}_c^T \mathbf{K}_c \Delta \mathbf{u}_c,$$

where  $\mathbf{F}_c$  is the contact force vector,  $\delta \mathbf{u}_c^T$  is a displacement vector for the contact

elements and  $\mathbf{K}_c$  is the contact stiffness matrix of the contact element containing the tangent stiffness matrix  $\mathbf{K}_N$  for the normal contact [35].

Taking all of the above into consideration, the final global nonlinear element equation for penalty approach is as follows:

$$(2.3) \quad \mathbf{M}\ddot{\mathbf{U}} + [\mathbf{K} + \mathbf{K}_c]\mathbf{U} = \mathbf{F}(t) - \mathbf{F}_c,$$

where  $\mathbf{M}$  is the mass matrix,  $\mathbf{K}$  is the stiffness matrix and vector  $\mathbf{F}(t)$  describing external force.

It should be concluded that the most challenging problem in this approach is the contact stiffness assessment, which, as it will be discussed in the next section of the paper, is dependent on many factors.

**2.2. Penalty contact implementation in explicit code**

In SPH and FEM, the contact process played a significant role due to its direct influence on the interaction between the shaper and bars (striker and incident) as well as on the obtained impulse shape. Thus, it was necessary to simulate the interaction between the segments of collaborating parts as accurately as possible. In explicit software, the interaction between two or more bodies is defined using the so-called penalty function approach [36, 37, 38]. For parts with different stiffness, contact stiffness is determined by the following formula:

$$(2.4) \quad k_{cs}(t) = 0.5 \cdot SOFSCL \cdot m \cdot \left( \frac{1}{\Delta t_c(t)} \right),$$

where *SOFSCL* – scaling factor, *m* – function dependent on masses of master and slave nodes,  $\Delta t_c$  – initial time step dependent on the contact procedure (if the solution time step grows,  $\Delta t_c$  is reset to the current time step to prevent unstable behaviour of the simulation).

In the above formula, it is possible to observe that the contact stiffness depends, inter alia, on  $\Delta t_c$ , which, in turn, directly influences the solution time step and can be placed in the following formula:

$$(2.5) \quad \Delta t = C \min(\Delta t_c, \Delta t_{FE}),$$

where  $\Delta t_c$  – time step size dependent on the contact procedure,  $\Delta t_{FE}$  – time step size based on the discrete element (selected from all elements in the model), *C* – scale factor related to the CFL stability condition.

**2.3. MM-ALE coupling modelling**

In the modelling of coupling in MM-ALE, the penalty based method is also used (or constraint based method, which preserves momentum, however does not conserve energy). In this case, the fictional elastic element is also defined

between interacting nodes. The value of its stiffness is calculated based on the minimum stiffness of elements being in contact.

In the matrix approach, a coupling process can be described using a general equation for a gaseous (liquid) medium  $f$  [39]:

$$(2.6) \quad M_f \dot{v} + N(v - \dot{\chi})v + K_f v + B_f p = R_f + F_f$$

and a solid medium  $s$ :

$$(2.7) \quad M_s \ddot{u} + K_s(u)u = R_s + F_f,$$

where  $p$  – pressure,  $F_f$  – coupling force,  $R_f$ ,  $R_s$  – external forces,  $K_f$  – viscosity,  $B_f$  – differential operators matrix,  $N$  – nonlinear part dependent on the difference between velocity of MM-ALE system configuration and velocity of Eulerian gas.

Moreover, within the boundary of two mediums (gaseous or liquid and solid) the following equilibrium condition must be satisfied [39]:

$$(2.8) \quad F_f v = F_s \dot{u},$$

where  $v$  – velocity of gaseous (liquid) medium,  $\dot{u}$  – velocity of solid medium.

### 3. Methodology of experimental and numerical studies

#### 3.1. Experimental set-up background

A classical compression split Hopkinson pressure bar was applied in the present studies. The apparatus presented in Fig. 2 consists mainly of a striker launching system (air pressure gun), a striker, an incident bar, a transmission bar (bar system), a velocity measuring device and a computer-controlled high-frequency data acquisition system. The incident bar and the transmission bar were  $1218 \pm 0.25$  mm long each, while the striker length was  $200 \pm 0.05$  mm. Both the bars and the striker had a diameter of 12.05 mm and were made of commercial maraging steel grade 350, which was heat treated to guarantee a high strength property of bars (nominal quasi-static yield strength  $R_{0.2} = 2320$  MPa, Young modulus  $E = 190.6$  GPa, sound speed  $C_0 = 4866$  m/s). Each bar was supported by four linear bearing stands, which were mounted on an optical bench allowing precise alignment of the bars system.

The elastic deformation signals in the incident and transmitted bars were captured using a pair of strain gauges attached symmetrically on the opposite surfaces of the bars and in the middle of their length. The strain gauges were connected to the opposite legs of the Wheatstone bridge, which was a typical half-bridge configuration. On the other legs of the bridge, the dummy resistors were mounted, resistance of which matched the strain gauges resistance. The typical

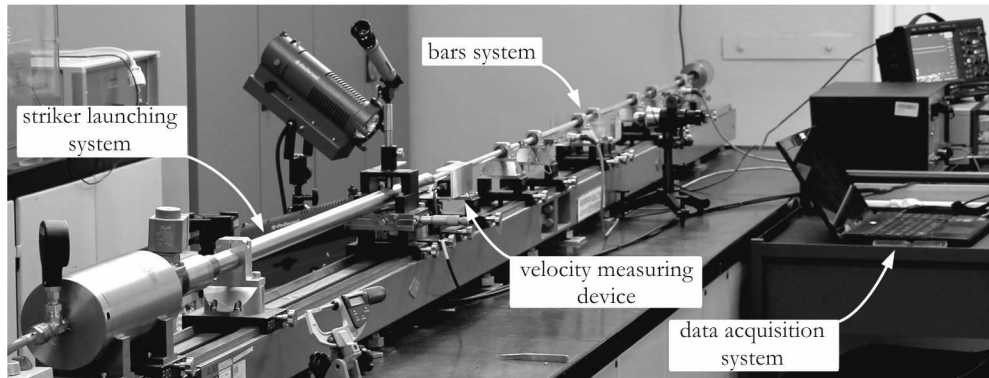


FIG. 2. Split Hopkinson pressure bar (SHPB) used in investigations.

electrical strain gauges of 1.6 mm were used (CEA-13-062UW-350, Vishay Micro-Measurements). The amplified signals of the strain gauges were recorded with a frequency of 1 MHz with the use of the signal conditioning unit (SGA-0B V5 Wheatstone bridge with signal conditioning amplifiers, ESA Messtechnik) and the data acquisition system (LeCroy WJ354A high-speed digital oscilloscope). The conditioner utilized in tests can use different low-pass filters with the cut-off frequencies equal to 100 kHz, 200 kHz, 500 kHz and 1 MHz. In the presented investigations the 1 MHz filter was used. An example of raw signals (without pulse shaper and specimen) from the strain gauges conditioned with the applied measuring equipment is shown in Fig. 3.

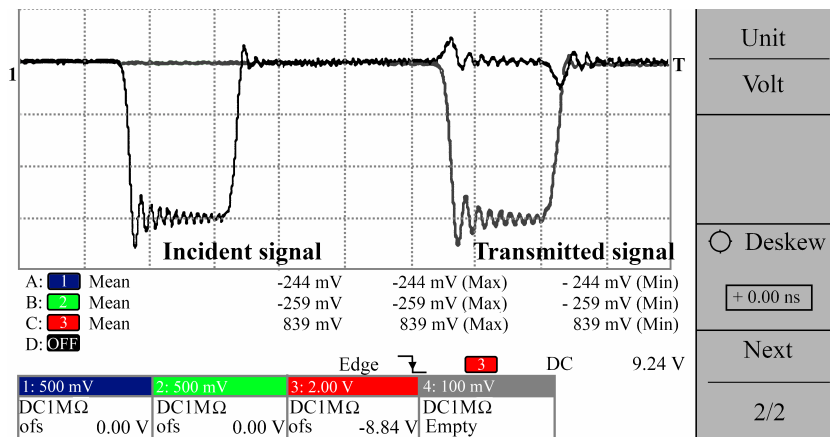


FIG. 3. Raw incident and transmitted wave signals measured by strain gauges.

Before testing, the SHPB apparatus was calibrated by checking if the relationship between the actually measured strain in the incident bar and the pre-

dicted signal amplitude related to the striking velocity was satisfied. In order to measure the impact velocity of the striker with the satisfactory accuracy, a Micro-Epsilon optoCONTROL1200 laser-beam measurement system was utilized. The data processing and analyses were carried out using programs developed in the Mathcad environment.

Discs of 5.56 mm diameter made of Cu-ETP copper sheet were used as pulse shapers. The pulse shapers were manufactured from 0.32 mm copper sheet with the use of a sheet metal punching technique.

### 3.2. Numerical methodology

The authors focused only on the copper shaper modelling using different methods and incident pulse assessment; thus, specimen, stopper and transmission bar were omitted. In all cases three-dimensional model was used instead of axial symmetric. The latter is less computationally expensive but the 3D model will give the possibility to study additional problems such as non-axial impacts of striker, discontinuity in bars or poor quality of specimen or bars. These kinds of analyses are going to be also performed in the next steps and their influence on the results will be also investigated. A more detailed description of SHPB apparatus modelling can be found in the authors' previous paper [28].

Numerical simulations within the presented study were performed using an aforementioned explicit solver with a central difference scheme and with the implementation of a modified equation of motion time integration [35]. In the carried out analyses, the stability of computations was guaranteed by Courant–Friedrichs–Lewy (CFL) condition, which states that the time step must be less than a certain time, otherwise the simulation will produce incorrect results [37]:

$$(3.1) \quad C = \frac{u_x \Delta t}{\Delta x} + \frac{u_y \Delta t}{\Delta y} + \frac{u_z \Delta t}{\Delta z} \leq C_{\max},$$

where  $u_x, u_y, u_z$  are velocities,  $\Delta t$  is the time step,  $\Delta x, \Delta y, \Delta z$  are length intervals,  $C_{\max}$  varies with the method used (in presented investigations, it was set to  $C_{\max} = 0.66$ , which is recommended for strongly dynamic phenomena).

**3.2.1. FE shaper modelling.** In FE modelling, in order to simplify and shorten computational time, symmetry of the problem was assumed and only a quarter of the model was taken into consideration. Dimensions and initial-boundary conditions directly corresponded to the experimental ones. As it was stated before, a copper pulse shaper, modelled using Lagrangian elements, was placed between the striker and the incident bar (Fig. 4). The striker and incident bar consisted of fully integrated hexagonal elements with a number of 4600 and 35 075, respectively. Also, it should be noted that the number of elements did not affect the results, which was confirmed in parallel tests.

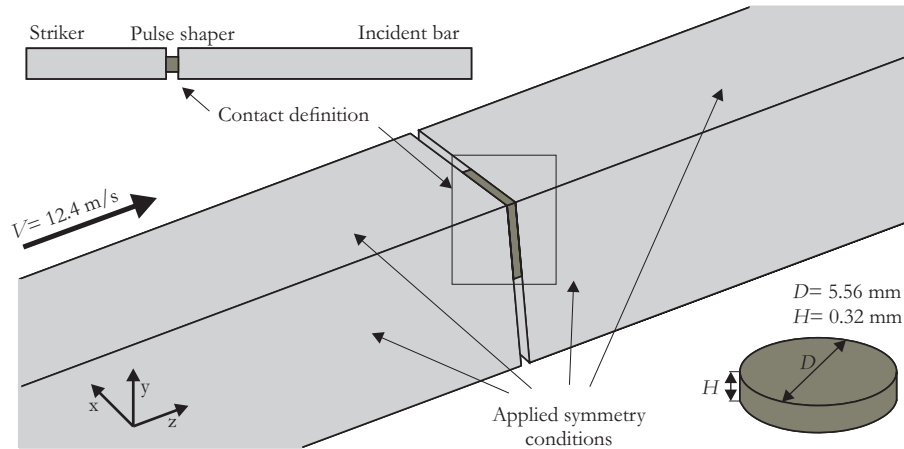


FIG. 4. Initial-boundary conditions applied in numerical analyses in FE shaper modelling.

For the copper pulse shaper, fully integrated hexagonal elements were used. The shape of elements was selected in order to guarantee the accuracy and stability of computations throughout analysis in which the copper wave shaper becomes largely compressed. As it was mentioned before, one of the main tasks was to perform a sensitivity study of mesh density, which varied from the coarser to the finer one. The authors decided to choose three different cases (Fig. 5):

- pulse shaper modelled using 300 elements and 465 nodes,
- pulse shaper modelled using 775 elements and 1074 nodes,
- pulse shaper modelled using 1368 elements and 1799 nodes.

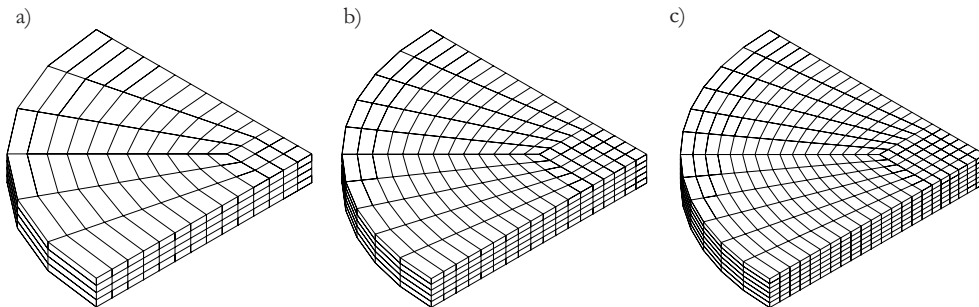


FIG. 5. Three different mesh densities of FE copper shaper used in analyses.

The interaction between the striker, the bar and the shaper was described by the surface to surface contact procedure and no friction was assumed, which in actual conditions is practically zero and is provided by lubricating contact surfaces. In FE simulations a pinball segment based contact was applied (*SOFT 2*).

The scale factor for constraint force was set to 0.12 and warped segment checking as well as sliding option were enabled ( $SBOPT = 5$ ). Search depth was set to the value of 2 (improved accuracy) and the number of cycles between the bucket sort was set to 15.

**3.2.2. SPH shaper modelling.** In the SPH case, the shaper and the bars had the same dimensions as previously, the problem symmetry was also assumed and only a quarter of the model was taken into consideration (identical initial-boundary conditions and a number of finite elements forming the bars). The interaction between the SPH shaper, the Lagrangian striker and the bar was described by the nodes to surface contact procedure (without friction). Here, the soft constraint formulation was applied ( $SOFT\ 1$ ) with the scale factor for constraint force set to 0.11. Search depth and the number of cycles between the bucket sorts were the same as in the FE simulations.

It should be pointed out that the bulk viscosity is a very significant parameter in SPH modelling, which prevents interparticle penetration and allows shocks to form and to damp post-shock oscillations. Moreover, it was found that default values for the artificial bulk viscosity for FE solid elements are not appropriate when SPH particles are used in such a kind of simulation [40]. Thus, in the presented investigations, the authors used values recommended in [40] for SPH formulation:  $Q_1 = 1.5$  and  $Q_2 = 1.0$ . Three SPH models with different number of particles (similar to elements number in previous case) were also analysed (Fig. 6):

- a) pulse shaper modelled using 280 particles,
- b) pulse shaper modelled using 665 particles,
- c) pulse shaper modelled using 1324 particles.

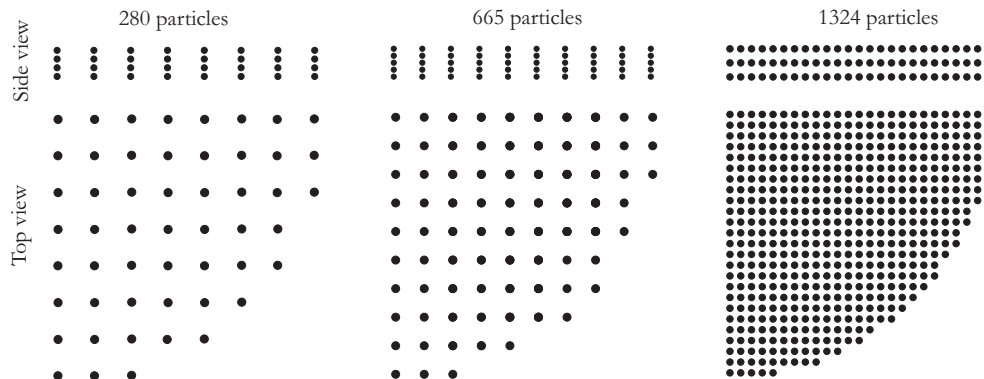


FIG. 6. Three different numbers of particles in SPH copper shaper used in analyses.

**3.2.3. MM-ALE shaper modelling.** In the MM-ALE case, the shaper had the same dimensions as previously and also identical striker velocity was applied. The wave shaper was described with Eulerian formulation, whereas both the striker and the bar were modelled using Lagrangian elements. The shaper was placed inside the Euler domain (vacuum) and no symmetry conditions were assumed (Fig. 7). The interaction between the Eulerian shaper, vacuum domain and Lagrangian parts was described using the penalty coupling procedure with the Van Leer second-order advection method [40]. It should be also pointed out, that in MM-ALE simulations a fine and regular mesh is desired. Therefore in the presented case, a large number of elements (with the smallest element length equals to  $\sim 0.05$  mm in the case c) were used, which resulted in long-lasting computations.

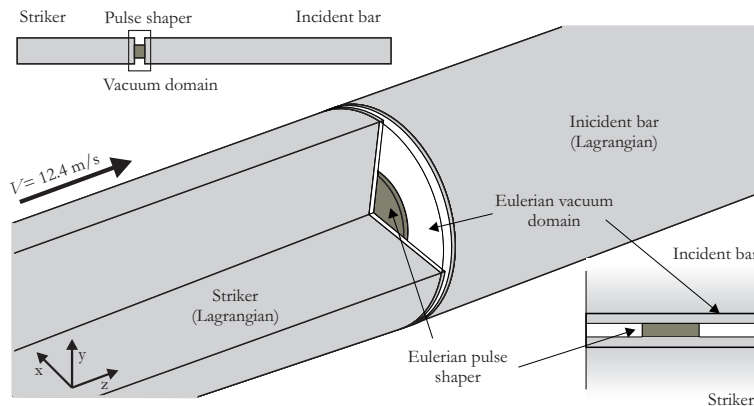


FIG. 7. SHPB with wave shaper in MM-ALE modelling.

Similarly to previous cases, three different mesh densities were also used and compared (Fig. 8):

- a) pulse shaper modelled using 1520 elements and 2005 nodes,
- b) pulse shaper modelled using 2640 elements and 3318 nodes,
- c) pulse shaper modelled using 9120 elements and 10927 nodes.

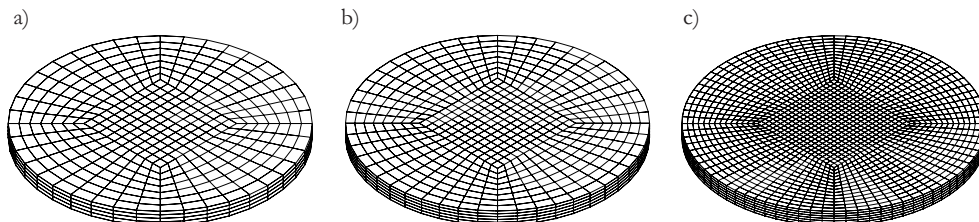


FIG. 8. Three different mesh densities in MM-ALE copper shaper used in analyses.

#### 4. Material properties definition

Material properties for the bars were described with typical Hooke's law elastic constitutive model (with literature steel data) since the incident and striker bar remain elastic during tests [1]. It is well known that the maximum stresses rise with strain rates, which also influences yielding of a material [10]. In the presented studies, the copper shaper deforms under dynamic conditions where strain rate plays a significant role (the viscous effects are initiated in the material). Thus, in all cases of wave shaper modelling (FE and SPH), the Johnson–Cook constitutive material model was utilized (Table 1). It provides a prediction of flow stress  $\sigma_{\text{flow}}$  for large strains and high strain rates, where its dependence on strain rate is linear in a semilogarithmic scale [37, 41]:

$$(4.1) \quad \sigma_{\text{flow}} = [A + B(\varepsilon^p)^n](1 + C \ln \dot{\varepsilon}_*^p),$$

where  $A, B, C, n$  – material constants,  $\varepsilon^p$  – effective plastic strain,  $\dot{\varepsilon}_*^p$  – effective plastic strain rate.

**Table 1. Properties of copper for the J-C constitutive material model used in analyses [37, 41].**

$A$ [MPa]	$B$ [MPa]	$N$ [-]	$C$ [-]	$\rho$ [kg/m <sup>3</sup> ]	$E$ [MPa]	$\nu$ [-]
92	292	0.310	0.025	1.09	115 000	0.33

**Table 2. Constants required for input in the Grüneisen EOS [42].**

$C_0$ [m.s]	$S_1$ [-]	$S_2$ [-]	$S_3$ [-]	$\gamma_0$ [-]	$A$ [-]
3933	1.5	0	0	1.99	0.5

The Grüneisen equation of state was used for describing a pressure-volume relationship of the copper pulse shaper with constants taken from literature [42] (Table 2). It defines the pressure in compressed materials as [37]:

$$(4.2) \quad p = \frac{\rho_0 C^2 \mu \left[ 1 + \left( 1 - \frac{\gamma_0}{2} \right) \mu - \frac{a}{2} \mu^2 \right]}{\left[ 1 - (S_1 - 1) \mu - S_2 \frac{\mu^2}{\mu + 1} - S_3 \frac{\mu^3}{(\mu + 1)^2} \right]^2} + (\gamma_0 + a \mu) E$$

and for expanded materials as [37]:

$$(4.3) \quad p = \rho_0 C^2 \mu + (\gamma_0 + a \mu) E,$$

where  $C$  – intercept of  $v_s$ - $v_p$  curve (shock wave velocity vs. particle velocity),  $S_1$ ,  $S_2$ ,  $S_3$  – coefficients of the slope of  $v_s$ - $v_p$  curve,  $\gamma_0$  – Grüneisen gamma,  $a$  – first order volume correction to  $\gamma_0$ , and  $\mu = \rho/\rho_0 - 1$ .

## 5. Results and discussion

### 5.1. Validation results

As it was mentioned before, the main aim of investigations is to present the possibility of copper shaper numerical modelling using different methods with the additional mesh sensitivity study. First, however, a developed numerical model of SHPB was validated with the actual one by comparing the raw incident pulse, without using any pulse shaping. Also, three different striker velocities:  $v_1 = 11.2$  m/s,  $v_2 = 9.8$  m/s,  $v_3 = 6.7$  m/s were used, which ensured that material parameters and initial-boundary conditions were proper. All tests were performed on the SHPB presented earlier. During tests no material characteristics were investigated, thus the transmission bar (transmitted pulse) and the copper shaper were not taken into consideration. From simulations, the incident impulse (axial stress:  $\sigma_{zz}$ ) was taken from the incident bar element which directly corresponded to the place where the strain gauge was glued.

It can be observed that all three incident impulses obtained during analyses are coincident with the experimental ones, thus an FE model of SHPB can be considered as validated. Moreover, it can be also observed that the shape of a contact force impulse between the bars and the corresponding incident pulse is nearly identical for all three cases. Thus, it is clearly confirmed that the shape of the elastic wave, which travels through bars, is directly related to the contact procedure between the simulated bodies (Figs. 9–11). At this point it should be noted that defining the contact stiffness should be carried out very carefully (its parameters) as it can change results drastically even for the same initial-boundary conditions.

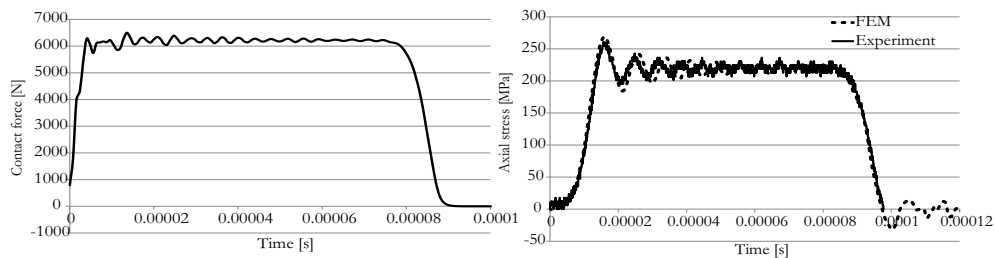


FIG. 9. Contact force and numerical incident pulse with experimental comparison for  $v_1 = 11.2$  m/s.

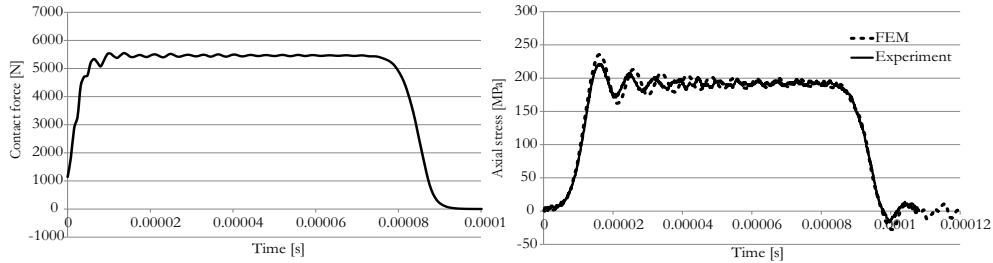


FIG. 10. Contact force and numerical incident pulse with experimental comparison for  $v_1 = 9.8$  m/s.

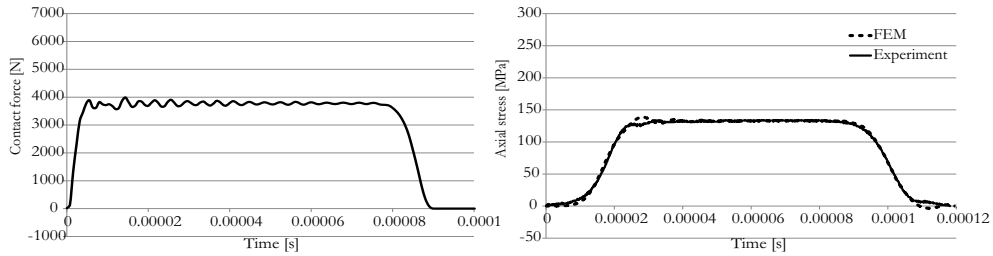


FIG. 11. Contact force and numerical incident pulse with experimental comparison for  $v_1 = 6.7$  m/s.

## 5.2. Experimental test with copper shaper results

In the next steps, a pulse shaper made of copper (5.58 mm diameter, 0.32 mm thickness) was placed between the striker and the incident bar. Similarly to the validation tests, three different striker velocities were used:  $v_{1s} = 12.4$  m/s,  $v_{2s} = 8.3$  m/s and  $v_{3s} = 7.2$  m/s. It should be noted that the authors' intention was not to compare pulses with and without the shaper, therefore the velocity values are not identical with those in validation tests, however, a certain similarity can be noticed. As a result, the incident pulses were obtained (Fig. 12), which, as it can be observed, are different than those without a wave shaper (Figs. 9–11). The main and most visible differences are: increased rise time, pulse length and lack of oscillations.

The authors decided that the most representative case to investigate is the case with the highest velocity. Such choice was dictated by the fact that the copper shaper was tested under the most extreme conditions due to the maximum deformation during dynamic compression between the bars. Thus, the authors assumed that if the obtained results are proper for such conditions, they will be also correct for the lowest velocities. Apart from geometrical changes, a shaper effect on the incident pulse was also investigated, which directly influ-

ences material behaviour during tests. It is well documented [1, 5, 17–20] that a “streamlined” impulse shape gives the possibility to obtain stress equilibrium in a specimen (for the specific family of materials) and sometimes constant strain rate conditions during tests. If those two parameters are satisfied, the tests can be considered as ideal and correctly carried out.

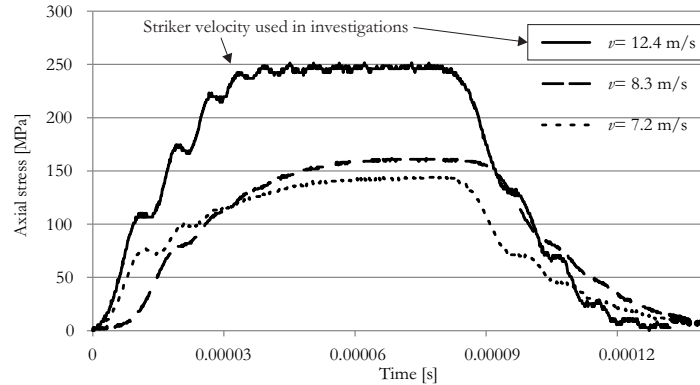


FIG. 12. Incident pulses obtained from experimental tests.

### 5.3. Numerical analyses with copper shaper results

In the paper, the main aspect of investigations was to compare the results of the obtained incident pulse shape and copper shaper deformation for different numerical methods and mesh (particles) densities. Additionally, numerical impulses were compared with the experimental one.

In Fig. 13, deformation of the shaper made of FE is shown for three different mesh densities (for better visualization, the quarter of the model was reflected in two directions). It can be observed that for the coarsest mesh the smallest diameter and greater height was obtained, whereas the finest mesh resulted in the largest deformation of the shaper. Moreover, abnormal deformation of elements within the symmetry boundary is clearly noticed. It resulted from the fact, that nodes of these elements have constraints on the normal direction of the symmetry plane ( $ZX$  and  $ZY$ ). Moreover, in the presented investigations hexagonal elements with three degrees of freedom on their nodes were also used [37].

Shaper deformation for SPH models (reflected in  $ZX$  and  $ZY$  direction) is presented in Fig. 14, also for three different numbers of particles. In this case, the measurement of the diameter and height was problematic, due to the fact that for the SPH generation the “cylinder” method was used instead of other, e.g., generating particles on hexagonal nodes. Such a choice was dictated by one of the main conditions for a proper SPH simulation, according to which the mesh must be as regular as possible and must not contain too large variations [36]. Similarly

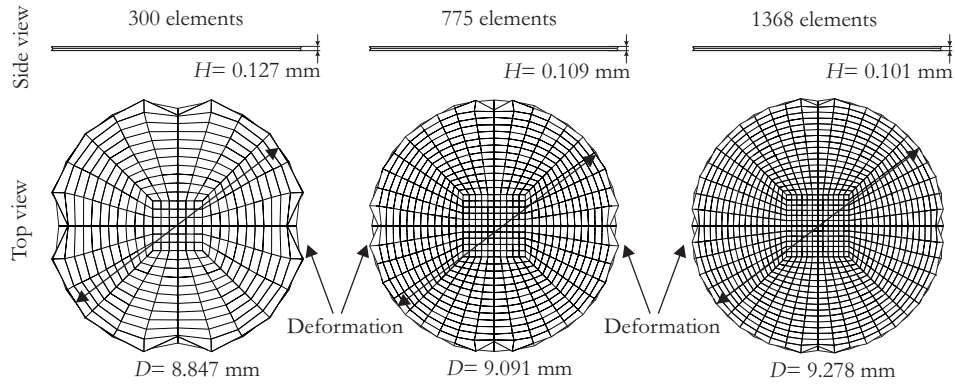


FIG. 13. Copper shaper deformation (max. compression) comparison for all FE cases.

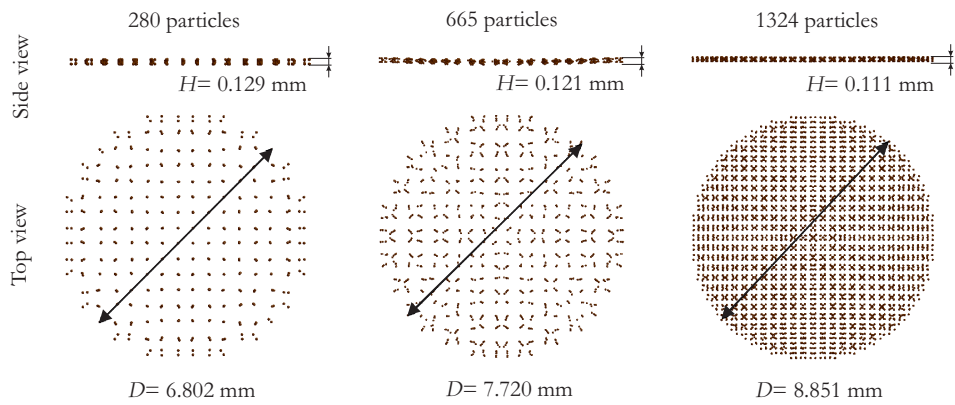


FIG. 14. Copper shaper deformation (max. compression) comparison for all SPH cases.

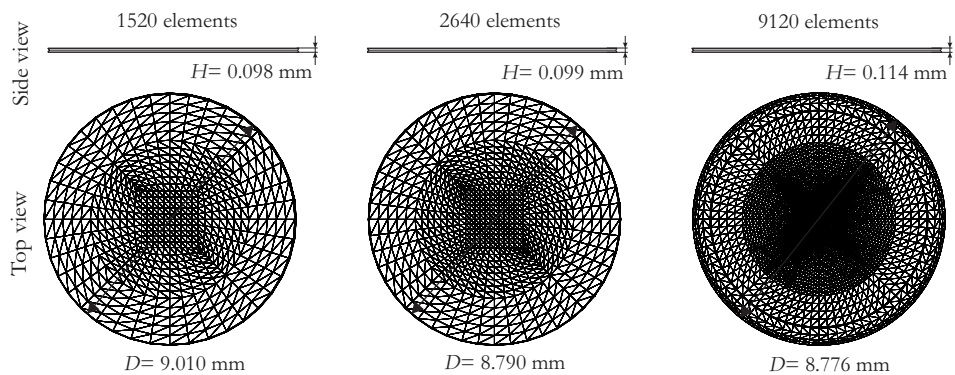


FIG. 15. Copper shaper deformation (max. compression) comparison for all MM-ALE cases.

to previous FE results, the more particles the larger deformation of the shaper was obtained. Nevertheless, the SPH shaper is stiffer than a Lagrangian model: the maximum diameter in FE was  $\sim 9.278$  mm, whereas in SPH  $\sim 8.851$  mm. This is caused by the fact that each element formulation handles deformation, and consequently, stresses in different way [37].

Figure 15 presents the results from analyses with MM-ALE formulation. Contrary to previous cases, the smaller number of elements resulted in a larger diameter and smaller height of the copper shaper. Although diameters were nearly the same as for the FE modelling and slightly different from the SPH technique, the shaper was more compressed (FE min. height:  $\sim 0.101$  mm, SPH:  $\sim 0.111$  mm, MM-ALE:  $\sim 0.098$  mm). The authors suppose that the main reason of such phenomena is the fact that in MM-ALE simulation the copper shaper is treated as a fluid (gas), thus it is much more compressible than both Lagrangian and SPH model.

Moreover, by comparing a diameter and length after the impact with the actual shaper used in experiments, a good correlation between the results can be observed (Table 3). Nevertheless, as it was mentioned before, SPH modelling differs slightly more from the experimental results as well as two other methods. However, as it will be presented in the further part of the work, an incident impulse curve for this method is the smoothest one.

**Table 3. Shaper dimensions after impact comparison.**

Experiment		Mean diameter [mm]	Height [mm]
		$\sim 8.600$	$\sim 0.130$
	No. of elements/particles	Diameter [mm]	Height [mm]
FEM	a) 300	8.847	0.127
	b) 775	9.091	0.109
	c) 1368	9.278	0.101
SPH	a) 280	6.802	0.129
	b) 665	7.720	0.121
	c) 1324	8.851	0.111
MM-ALE	a) 1520	9.010	0.098
	b) 2640	8.790	0.099
	c) 9120	8.776	0.114

Finally, the measured incident impulse characteristics (stress) were examined and compared (Figs. 17–19). In the simulations, pulse characteristics were taken from the incident bar finite element which position directly corresponded to the place where a real strain gauge was glued.

Firstly, the contact forces are presented in Fig. 16 for the three cases with the smallest number of elements (or particles). Reasonable correlation can be

noticed when comparing them with the incident pulse shapes for the corresponding methods. Nevertheless, softer material of the pulse shapers resulted in “smoother” rise and fall of the impulse amplitude in comparison to the validation tests (Figs. 9–11). Therefore, the same conclusion as previously arises: despite different methods of stiffness calculation between interacting bodies, contact force has a direct impact on the shape of an incident pulse.

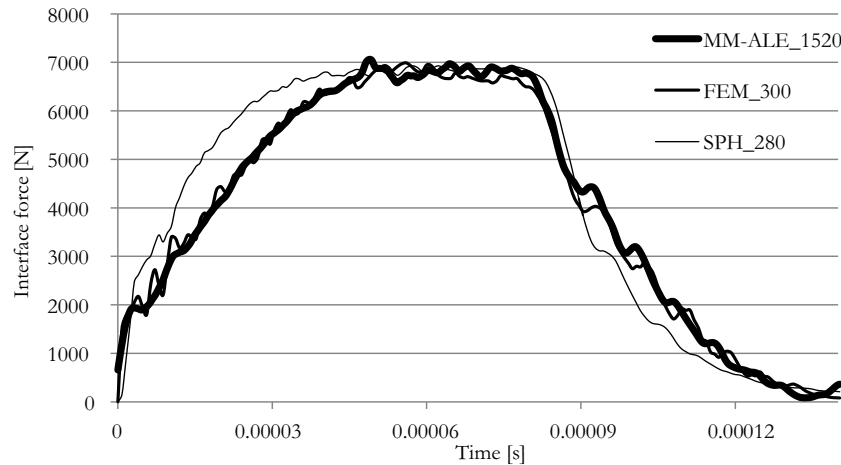


FIG. 16. Contact force comparison for different numerical methods.

As it was expected from the previous results showing deformation, a quite good agreement can be found for all FE three cases. In SPH modelling, it is possible to observe that a different number of particles resulted in slightly different characteristics: the rise times differ from each other, what is caused by various stiffness of the shaper for a different number of particles. In MM-ALE analyses, it may be observed that the smoothest curve was obtained for the coarsest mesh.

The authors assume that better correlation between experimental and numerical impulses could be obtained with proper material parameters estimated during dynamic compression testing on the SHPB.

In Fig. 20, chosen impulses from analyses (SPH with 280 particles and the coarsest FE and MM-ALE mesh) were compared with the experiment. All four impulses are characterized by nearly the same duration time which, from the physical point of view, is correct and also shows that the following formula is satisfied [1–3, 8, 14, 15]:

$$(5.1) \quad T = \frac{2L}{c_p},$$

where  $T$  the impulse duration time,  $L$  is the striker length and  $c_p$  is the elastic wave propagation velocity in the bar material.

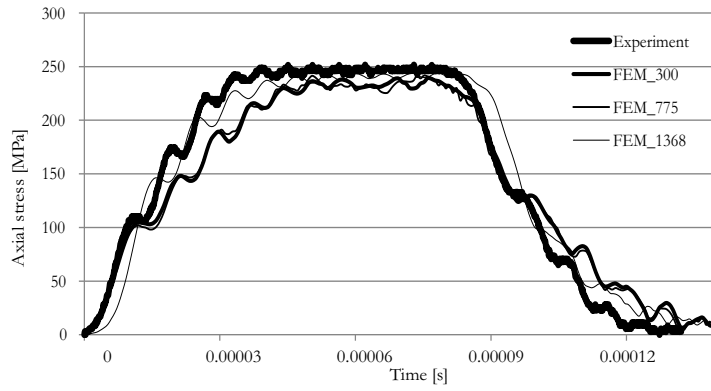


FIG. 17. Incident impulses obtained in FE shaper modelling and experimental test – comparison graph.

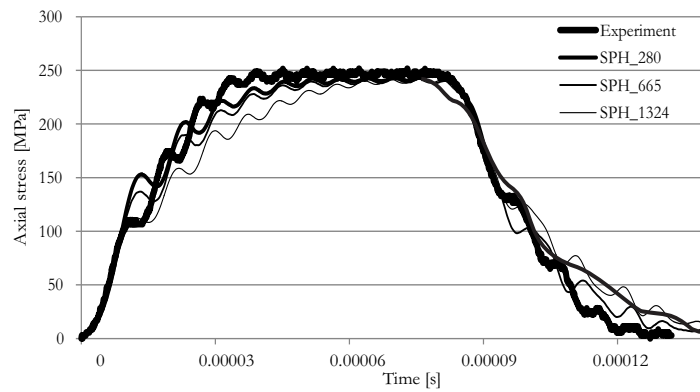


FIG. 18. Incident impulses obtained in SPH shaper modelling and experimental test – comparison graph.

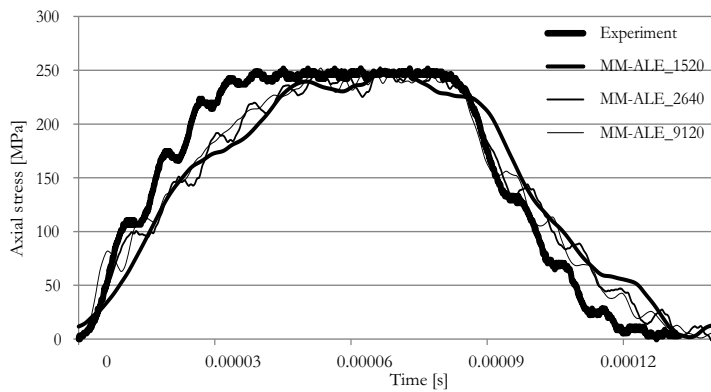


FIG. 19. Incident impulses obtained in MM-ALE shaper modelling and experimental test – comparison graph.

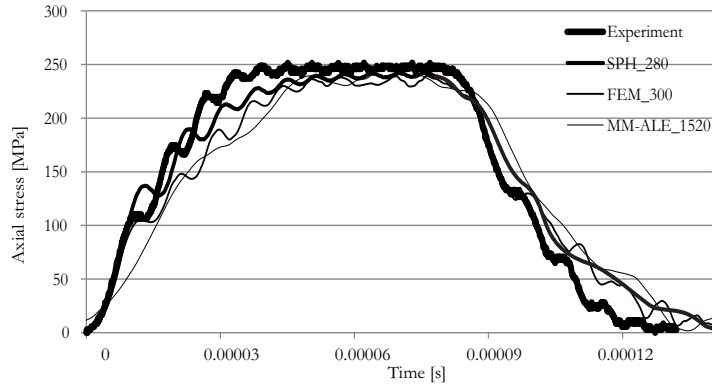


FIG. 20. Incident impulses obtained in three chosen cases from different shaper modelling methods compared to the experimental test.

It should be noted that despite the different modelling methods a similar behaviour of the shaper during the simulations was observed, with very small differences between the generated shape of the impulse and the maximum values of stress.

It is worth emphasizing the effectiveness of the implemented methods (for the finest mesh and a larger number of particles). MM-ALE formulation, due to the complex mathematical background and a large number of elements used, is the most computationally expensive – the analyses were carried out for 744 min. In fact, this was also caused by the low value of time step ( $\Delta t = 3.71e^{-9}$  s), which was basically dependent on the smallest element length (the smallest element length equals to  $\sim 0.05$  mm in the case with 9120 elements).

For the Lagrangian modelling, the simulation of the shaper ended after 62 min, whereas in SPH it took 11 min. In the first case, a time step varied due to the large elements deformation as well as contact calculation: the approximate value equalled to  $\Delta t = 9.65e^{-9}$  s. In the meshless analysis, the time step was approximately 3.5 times greater than in FE simulation, which is clearly reflected in computational time. Described information is listed in Table 4.

Table 4. Computational cost of the three methods (on the example of chosen cases).

	Time step [s]	Computational time [min]
FEM 1368 elements	$9.65e^{-9}$	$\sim 62$
SPH 1324 particles	$2.77e^{-9}$	$\sim 11$
MM-ALE 9120 elements	$3.71e^{-9}$	$\sim 744$

## 6. Conclusions

The paper presents the investigations of material testing at high strain rates and the study of constitutive models implementation under strongly dynamic simulations. One of the authors' main aims was also to present numerical modelling of SHPB testing with the principal attention paid to a copper shaper mesh (particles) sensitivity study with the assessment of its influence on the obtained incident pulse characteristics. Explicit analyses were carried out using a commercial explicit code with three different techniques used for modelling the shaper: typical finite element formulation (FEM), meshless smoothed particles hydrodynamics (SPH) method and multi-material arbitrary Lagrangian–Eulerian (MM-ALE) formulation. Moreover, the major aspect of the study was to highlight the importance of a correct contact procedure, which is one of the most essential parameters in such investigations. As a consequence, the relationship between the interaction force and the impulse shape was investigated for all cases and presented in the paper.

It was confirmed that the shape of the elastic wave, which travels through bars, is directly related to the contact procedure between the simulated bodies. Thus, despite different methods of stiffness calculation between interacting bodies, contact force has a direct impact on the shape of an incident pulse. The authors would like to emphasize the fact that defining the contact stiffness (its parameters) should be carried out very carefully as it can change results drastically even for the same initial-boundary conditions.

Considering the results it can be stated that the FE mesh density in such analyses is of minor importance. Despite a different number of elements, the obtained stress characteristics (impulses) were nearly identical. Nevertheless, abnormal deformation of the elements within the symmetry boundary was clearly noticed. This fact indicates that the discrete model of the shaper should be developed carefully. The number as well as the shape of the elements should be selected in order to guarantee the accuracy and stability of computations throughout analysis in which the copper sample becomes largely compressed.

From the SPH modelling the following conclusions can be derived: the method is vulnerable to the regularity of particles distribution, “dimensions” of a modelled part depends on a number of particles, a different number of particles resulted in slightly different values of obtained maximum stresses, a bulk viscosity parameter (with a specific SPH formulation) is very important in such strongly dynamic phenomena, where the continuity of material is of great importance and finally a well-developed model guarantees a very short lasting simulation.

In FE and SPH case, the contact algorithm applied using soft constraint option with modified parameters (contact stiffness is based on the nodal masses

and a global time step size) worked properly and guaranteed the absence of penetration.

In the most sophisticated of the used methods, i.e., MM-ALE, also reasonable results were obtained. However, there is a need to spend a lot of time in preparing and developing the model for analyses. This technique is also computationally expensive and for such short-lasting simulations of SHPB, time needed to prepare a model and to “see” the results is disproportionate. Nevertheless, the main intention of the authors was to present the possibility of various methods which are possible to be implemented in such phenomena. All three presented methods, in terms of SHPB numerical testing, have some advantages and disadvantages, however, all in all, the FE modelling seems to be the most suitable and efficient method due to its simplicity and universality.

In order to achieve the proper numerical modelling, the authors, in their future studies, will also extend the investigations by including dynamic experimental tests of copper and other shaper materials for the exact constitutive parameters obtainment. It is worth noting that the presented study is a part of wider investigations of finding an ideal shape of an incident pulse for brittle, ductile or soft material. It will result in a possibility to perform experimental tests under constant strain rate conditions and with stress equilibrium in a specimen.

### Acknowledgements

The research was carried out under a research grant no. RMN 723. This support is gratefully acknowledged.

### References

1. S. ELLWOOD, L.J. GRIFFITHS, D.J. PARRY, *Materials testing at high constant strain rates*, Journal of Physics E: Scientific Instruments, **15**, 280–282, 1982.
2. J. HOPKINSON, *On the rupture of iron wire by a blow*, Proc. Literary and Philosophical Society of Manchester, 40–45, 1872.
3. B. HOPKINSON, *The effect of momentary stress in metals*, Proc. of the Royal Society of London, 498–507, 1905.
4. C.M. ROLAND, *Mechanical behaviour of rubber at high strain rates*, Rubber Chemistry and Technology, **79**, 429–459, 2006.
5. B. SONG, W. CHEN, *Split Hopkinson pressure bar techniques for characterizing soft materials*, Latin American Journal of Solid and Structures, **2**, 113–152, 2005.
6. W. CHEN, F. LU, D.J. FREW, M.J. FORRESTAL, *Dynamic compressive testing of soft materials*, Journal of Applied Mechanics, **69**, 214–223, 2002.
7. T. IWAMOTO, T. NAGAI, T. SAWA, *Experimental and computational investigations on strain rate sensitivity and deformation behavior of bulk materials made of epoxy resin structural adhesive*, International Journal of Solids and Structures, **47**, 2, 175–185, 2010.

8. D.J. PARRY, A.G. WALKER, P.R. DIXON, *Hopkinson bar pulse smoothing*, Measurement Science and Technology, **6**, 443–446, 1995.
9. J. JANISZEWSKI, *The study of engineering materials under dynamic loading*, Military University of Technology, Warsaw, 2012 [in Polish].
10. R. CHMIELEWSKI, L. KRUSZKA, W. MŁODOŻENIEC, *The study of static and dynamic properties of 18G2 steel*, Bulletin of MUT, **53**, 31–45, 2004 [in Polish].
11. E.A. PIECZYSKA, R.B. PECHERSKI, S.P. GADAJ, W.K. NOWACKI, Z. NOWAK, M. MATYJEWski, *Experimental and theoretical investigations of glass-fibre reinforced composite subjected to uniaxial compression for a wide spectrum of strain rates*, Archives of Mechanics, **58**, 3, 273–291, 2006.
12. J. HOPKINSON, *Further experiments on the rupture of iron wire*, Proc. Literary and Philosophical Society of Manchester, 119–121, 1872.
13. B. HOPKINSON, *A method of measuring the pressure produced in the detonation of high explosives or by the impact of bullets*, Philosophical Transactions of the Royal Society of London, **213**, 437–456, 1914.
14. R.M. DAVIES, *A critical study of the Hopkinson pressure bar*, Philosophical Transactions of the Royal Society of London, **240**, 375–457, 1948.
15. H. KOLSKY, *An investigation of the mechanical properties of materials at very high rates of loading*, Proc. of the Physical Society, **62**, 676–700, 1949.
16. K.F. GRAFF, *Wave motion in elastic solids*, Dover Publications, New York, 2004.
17. B. SONG, W. CHEN, *Dynamic stress equilibration in split Hopkinson pressure bar tests on soft materials*, Experimental Mechanics, **44**, 3, 300–312, 2004.
18. D.J. FREW, M.J. FORRESTAL, W. CHEN, *Pulse shaping techniques for testing brittle materials with a split Hopkinson pressure bar*, Experimental Mechanics, **42**, 1, 93–106, 2002.
19. J.R. FOLEY, J.C. DODSON, C.M. MCKINION, *Split Hopkinson bar experiments of preloaded interfaces*, Proc. of the IMPLAST 2010 Conference, 2010.
20. C.E. FRANZ, P.S. FOLLANSBEE, I. BERMAN, J.W. SCHROEDER, *High energy rate fabrication*, American Society of Mechanical Engineers, 1984.
21. T.J. CLOETE, A. V.D. WESTHUIZEN, S. KOK, G.N. NURICK, *A tapered striker pulse shaping technique for uniform strain rate dynamic compression of bovine bone*, EDP Sciences, 901–907, 2009.
22. H. RAMIREZ, C. RUBIO-GONZALEZ, *Finite-element simulation of wave propagation and dispersion in Hopkinson bar test*, Materials and Design, **27**, 36–44, 2006.
23. Z. PING YU, L. DE SHUN, P. YOU DUO, C. AN HUA, *Inverse approach to determine piston profile from impact stress waveform on given non-uniform rod*, Transactions of Non-ferrous Metals Society of China, **11**, 2, 297–300, 2001.
24. X.B. LI, T.S. LOK, J. ZHAO, *Dynamic characteristics of granite subjected to intermediate loading rate*, Rock Mechanics and Rock Engineering, **38**, 1, 21–39, 2005.
25. L.K. SENG, *Design of a new impact striker bar for material tests in a split Hopkinson pressure bar*, Civil Engineering Research Bulletin, **16**, 70–71, 2003.
26. L. WANG, M. XU, J. ZHU, S. SHI, *A method of combined SHPB technique and BP neural network to study impact response of materials*, Strain, **42**, 149–158, 2006.
27. P. BARANOWSKI, J. MALACHOWSKI, R. GIELETA, K. DAMAZIAK, L. MAZURKIEWICZ, D. KOŁODZIEJCZYK, *Numerical study for determination of pulse shaping design variables*

- in SHPB apparatus*, Bulletin of the Polish Academy of Sciences: Technical Sciences, **61**, 2, 459–466, 2013.
28. C.F. LEWIS, *Properties and selection: nonferrous alloys and pure metals*, Metals Handbook, American Society for Metals, 1979.
  29. H.G. BARON, *Stress/strain curves for some metals and alloys at low temperatures and high rates of strain*, The Journal of the Iron and Steel Institute, **182**, 354–365, 1956.
  30. D.J. FREW, *Dynamic response of brittle materials from penetration and split Hopkinson pressure bar experiments*, US Army Corps of Engineers, Engineer Research and Development Centre, 2001.
  31. R. NAGHDABADIA, M.J. ASHRAFIA, J. ARGHAVANI, *Experimental and numerical investigation of pulse-shaped split Hopkinson pressure bar test*, Materials Science and Engineering A, **539**, 285–293, 2012.
  32. F. BENASSI, M. ALVES, *Pulse shaping in the split Hopkinson pressure bar test*, Proc. from the IV National Congress of Mechanical Engineering, 2006.
  33. T. JANKOWIAK, A. RUSINEK, T. LODYGOWSKI, *Validation of the Klepaczko–Malinowski model for friction correction and recommendations on split Hopkinson pressure bar*, Finite Elements in Analysis and Design, **47**, 1191–1208, 2011.
  34. T. IWAMOTO, T. YOKOYAMA, *Effects of radial inertia and end friction in specimen geometry in split Hopkinson pressure bar tests: a computational study*, Mechanics of Materials, **51**, 97–109, 2012.
  35. P. WRIGGERS, T.V. VAN, E. STEIN, *Finite element formulation of large deformation impact-contact problems with friction*, Computers and Structures, **37**, 319–333, 1990.
  36. S. VULOVIC, M. ZIVKOVIC, N. GRUJOVIC, R.A. SLAVKOVIC, *Comparative study of contact problems solution based on the penalty and Lagrange multiplier approaches*, J. Serbian Society for Computational Mechanics, **1**, 1, 174–183, 2007.
  37. J.O. HALLQUIST, *LS-Dyna: Theoretical manual*, California Livermore Software Technology Corporation, 2003.
  38. P. BARANOWSKI, J. BUKALA, K. DAMAZIAK, J. MALACHOWSKI, L. MAZURKIEWICZ, T. NIEZGODA, *Numerical description of dynamic collaboration between rigid flying object and net structure*, Journal of Transdisciplinary Systems Science, **16**, 1, 79–89, 2012.
  39. H.G. MATTHIES, R. NIEKAMP, *Numerical and algorithmic aspects of coupled problems*, First South-East European Conference on Computational Mechanics, SEECCM-06, 31–38, 2006.
  40. L.E. SCHWER, *Aluminium plate perforation: a comparative case study using Lagrange with erosion, multi-material MM-ALE and smooth particle hydrodynamics*, Proc. from the 7th European LS-DYNA Conference, 2009.
  41. G.R. JOHNSON, W.H. COOK, *A constitutive model and data for metals subjected to large strains, high strain rate and high temperatures*, Proc. from the 7th International Symposium on Ballistics, 1983.
  42. D. STEINBERG, *Equation of state and strength properties of selected materials*, Lawrence Livermore National Laboratory, Livermore, CA, 1906.

Received January 15, 2014; revised version June 30, 2014.